Evaluation of Geostatistical Measures of Radiometric Spatial Variability for Lithologic Discrimination in Landsat TM Images

Francisco Abarca-Hernández and Mario Chica-Olmo

Abstract
Different measures of spatial variability (MSV) calculated from several estimators of the variogram function are used for lithologic discrimination in the framework of digital image classification. These measures are calculated in a local context using moving windows, which characterize the spatial variability of the radiometric data and represent textural indices to be used in image classification. Before applying this methodology, a spectral enhancement of the main geological features of the image by principal component analysis (PCA) has been necessary. The variographic analysis of the selected PCs in the training areas has shown important differences in the spatial behavior between lithologic classes. The MSV assessment was carried out by discriminant analysis in the training areas and supervised classification of the Landsat TM image. The results have shown that the use of TM radiometric data together with MSV improves the overall accuracy of the lithologic discrimination.

Introduction
Digital satellite imagery provides abundant multispectral information characterizing the interaction of electromagnetic radiation with terrestrial surface materials. This radiometric information is expressed by digital numbers that present spatial and temporal characteristics that usefully complement the study of natural resources.

In satellite image processing, digital classification is an important step to automatically categorize all the pixels in an image into land-cover classes or themes. In practice, the classical mathematical algorithms of supervised and non-supervised classification, mainly based on the application of pixel-by-pixel strategies, do not consider the spectral dependence existing between a pixel and its neighbors, i.e., spatial correlation. Therefore, the results obtained from pixel-by-pixel classifiers could be improved by taking into account additional information on the spatial autocorrelation of the digital numbers, jointly with the spectral data in the same classification strategy (Swain *et al.*, 1979). This improvement would arise as a consequence of the hypothesis that a pixel is not independent of its neighbors, and that this dependence can be quantified and incorporated into the classifier.

The autocorrelation or variability between pixels, which is related to the textural aspects of the image, can be characterized through spatial analysis of radiometric data (Abarca, 1997). Texture refers to the apparent roughness or local variability of the pixels, which is analyzed in practice by means of parameters that consider the spatial variation of the digital numbers, which can be obtained by considering either the whole image or by operating in a local moving window. Some of the most common textural descriptors are based on local statistical parameters (Sun and Qin, 1993), entropy (Haralick and Shanmugham, 1974), fractal dimension (Clarke, 1986), measures of the matrix of co-occurrence (Carlson and Ebel, 1995), and recent techniques that have involved the use of geostatistical parameters deduced from the variogram function (Carr, 1996; Lark, 1996).

This paper is intended to analyze the spatial dependence of radiometric data by geostatistical methods and include it in the classification algorithms. For this purpose, the digital number (DN) is interpreted as a regionalized variable (Matheron, 1965; Curran, 1988; Woodcock *et al.*, 1988), characterized by structural and random aspects, quantified by the variogram function. In our approach, the variogram calculation is made in a neighborhood using a moving window, enabling us to quantify the spatial variability of radiometric data at this local level. The experimental value of this function at a specific lag of distance h (in pixels) is assigned to the central pixel of the window, resulting in a geostatistical measure regarding the local textural character of the image. This measure represents a new variable to be used within the classification strategy.

This geostatistical methodology based on the analysis of the spatial dependence of the radiometry has been used to evaluate a set of measures of spatial variability (MSV) considering local textural indices. These measures are derived from the calculation of different geostatistical estimators of the variogram function, which are applied to the lithologic discrimination and classification of Landsat TM images.

Study Area and Satellite Images
The image used to illustrate the practical aspect of this study covers an area located in the southeast of Spain in the region of Cabo de Gata, province of Almería, Spain (Figure 1). Mineral exploration studies have traditionally been carried out in this area to map hydrothermal gold deposits, and, due to its environmental importance and unique landscapes, the region has been declared a Natural Park.

The geomorphologic modeling of the region is conditioned by the volcanic nature of the outcropping materials as well as by the typical plains of quaternary deposits associated with the erosion of the volcanic rocks in a semiarid climate. In a geological context, the main outcrops are neogene

Geodynamics Department/IACT. University of Granada, Av. Fuentenueva S/N, 18071 Granada, Spain (fabarca@carpanta.ugr.es, mchica@ugr.es).

Photogrammetric Engineering & Remote Sensing,
Vol. 65, No. 6, June 1999, pp. 705–711.

0099-1112/99/6506–705$3.00/0

Figure 1. Location of the study area in southeastern Spain.

volcanic materials of chalco-alkaline character, andesite, dacite, and rhyolite. These materials were subsequently affected by hydrothermal alteration processes intensified by the presence of fractures and fissures, with which important mineralizations of gold are associated (Arribas *et al.*, 1989). These predominant volcanic rocks sometimes present mineralogical compositions that are relatively alike, though the structural and textural aspects of their formation processes such as subvolcanic intrusions, ignimbrites, flows of volcanic material, domes, etc., are rather different. There also exist smaller quantities of important outcrops of tertiary materials represented by reef limestone deposits. Table 1 summarizes the main rocks outcropping in the study area, with their most noteworthy structural characteristics.

For this application, one Landsat TM subscene (07 July 1991) was selected in which a test area of 55 km^2 was taken (230 by 260 pixels) and was co-registered using the nearest neighbor method so as not to change the spatial autocorrelation structure of the digital numbers. No radiometric corrections were applied to the image because we preferred to retain the structure of the original data. This aspect does not represent any drawback because this methodology can also be applied to radiance or reflectivity data.

Table 1. Characteristics of Predominant Lithologies in the Study Area

Lithology	Main characteristics
Amphibole dacite	Domes of volcanic material outcropping as massive rocks.
Amphibole andesite	Subvolcanic intrusions formed by autoclastic breccias.
Rhyolite	Ignimbrites with variable texture.
Altered rhyolite and dacite	Domes formed by altered and fractured rocks.
Reef limestone	Reef limestone and bioclastic calcarenite. Miocene.
Quaternary deposits	Clays, sands, and conglomerates.

Methodology

The Variogram Concept

From a geostatistical point of view, the digital number of a satellite image is considered to be a regionalized variable (Curran, 1988; Atkinson, 1993; Chica-Olmo and Abarca, 1997). This variable is interpreted as a function $\mathrm{DN}(x)$ that provides the radiometric digital number DN of a pixel x located by its geographic coordinates or by its row and column in the image. The regionalized variable $\mathrm{DN}(x)$ behaves like a random variable, and "an image" may therefore be considered as a particular realization of the random function $\mathrm{DN}(x)$, which is composed of a set of random variables $[\mathrm{DN}(x_1), \mathrm{DN}(x_2), ..., \mathrm{DN}(x_n)]$ located at the pixels $x_1, x_2, ..., x_n$.

The intrinsic hypothesis leads to the semivariogram function concept, in practice also called variogram, which is expressed as (Matheron, 1971).

$$\gamma(h) = \frac{1}{2} E\{\mathrm{DN}(x) - \mathrm{DN}(x+h)\}^2 \tag{1}$$

where $\gamma(h)$ represents half of the mathematical expectation of the quadratic increments of pixel-pair values at a distance h. So, it is deduced that $\gamma(h)$ is a vectorial function depending on the modulus and the angle of the distance vector h between the pixels $x+h$ and x.

In image processing, the variogram is considered a powerful tool to analyze the regionalization of the radiometric data (Ramstein and Raffy, 1989). This term refers to the spatial variability characteristics of these data, and their study is usually based on the calculation, interpretation, and modeling of the experimental variogram. Variographic analysis is important because it provides valuable information about the variability of the radiometric data of the image at both a global and a local scale, and because it represents a measure of the textural features of the image used for lithologic discrimination by means of supervised classification.

Considering the raster structure of satellite imagery, the computing of the variogram does not represent any major difficulty, except that computing time could be lengthy depending on the size of the image. The interpretation of the variograms of the radiometric data is based on the knowledge of the lithologic aspects of the area, enabling us to deduce spatial variability parameters such as the range of the variogram, which is defined as the distance at which the spatial autocorrelation between digital data disappears; the behavior at the origin of the variogram, providing information on the degree of continuity of the digital numbers from small scale radiometric variations (nugget effect); and the spatial anisotropy, revealing different directional behavior in the distribution of the radiometric values. Furthermore, it is usual for the radiometric data to present different variability scales such that the overall variogram is defined by a sum of several elemental structures associated with different variation scales of the radiometric data.

The variogram modeling is required to fit the experimental variogram to a theoretical model. Journel and Huijbregts (1978) and McBratney and Webster (1986) provided a list of the most commonly used variogram models for variographic fitting: spherical, Gaussian, exponential, etc., but this process is only required in geostatistical applications in satellite image processing based on spatial estimation or conditional simulation (Atkinson *et al.*, 1994; Dungan *et al.*, 1994).

Measures of Spatial Variability (MSV)

The methodology used for the lithologic discrimination of Landsat TM images is based on the calculation of geostatistical measures of radiometric local spatial variability derived from the variogram function. In addition to Equation 1, representing the classical expression of the direct variogram, other expressions for estimators of spatial variability have also been proposed involving both the uni- and multivariate cases. In this study, the following five functions are considered: direct variogram, madogram, rodogram (Deutsch and Journel, 1992; Cressie, 1994) in the univariate case, and cross and pseudo-cross variograms (Wackernagel, 1995) in the multivariate one. All these experimental functions inform us about the local spatial variability of the radiometric data and represent a textural descriptor of the image that can be used for discrimination or classification purposes. The following spatial variability estimators have been used:

Direct Variogram (V)

The statistical inference of the direct variogram is obtained from the estimator of Equation 1: i.e.,

$$\gamma_k(h) = \frac{1}{2n(h)} \sum_{i=1}^{n(h)} \{dn_k(x_i) - dn_k(x_i + h)\}^2 \tag{2}$$

where $n(h)$ is the number of distant pairs h, dn (.) are the digital values of pixels x_i and $x_i + h$ and k is the sensor band.

Madogram (M)

The Madogram is similar to the direct variogram but, instead of squaring differences, the absolute difference is taken. This function is equivalent to the first-order variogram proposed by Matheron (1982): i.e.,

$$\gamma_k(h) = \frac{1}{2n(h)} \sum_{i=1}^{n(h)} | dn_k(x_i) - dn_k(x_i + h)| . \tag{3}$$

Rodogram (R)

The Rodogram is also similar to the direct variogram, but this considers the square root of the absolute difference instead of squaring differences: i.e.,

$$\gamma_k(h) = \frac{1}{2n(h)} \sum_{i=1}^{n(h)} \sqrt{| dn_k(x_i) - dn_k(x_i + h)|} . \tag{4}$$

Cross Variogram (CV)

The cross variogram quantifies the joint spatial variability (cross correlation) between two bands. It is defined as half of the average product of the h-increments relative to the radiometric bands j,k: i.e.,

$$\gamma_{jk}(h) = \frac{1}{2n(h)} \sum_{i=1}^{n(h)} \{[dn_j(x_i) - dn_j(x_i + h)] \cdot [dn_k(x_i) - dn_k(x_i + h)]\}. \tag{5}$$

Pseudo-Cross Variogram (PV)

The pseudo-cross variogram considers the variance of the cross increments instead of the covariance of the direct increments as above: i.e.,

$$\gamma_{jk}(h) = \frac{1}{2n(h)} \sum_{i=1}^{n(h)} \{[dn_j(x_i) - dn_k(x_i + h)] \cdot [dn_j(x_i) - dn_k(x_i + h)]\}. \tag{6}$$

For the application presented in this paper, the experimental computation of these measures of spatial variability was performed by calculating them within a neighborhood using moving windows of 7 by 7 pixels.

Selection of the Study Variables

The application of the above defined variograms has been done not on the original TM data but on variables transformed as below. For this purpose, two new variables were obtained from the radiometric information of the TM bands using principal component analysis (PCA) to characterize and highlight the spectral properties of the studied lithologic classes. These variables were obtained from the Feature Oriented Principal Component Selection (FPCS) method, proposed by Crosta and McMoore (1989) and later applied to hydrothermal alteration mapping by Loughlin (1991). This method is based on the detailed examination of the weights of the eigenvectors to determine the principal components best related to the theoretical spectral signatures of the studied lithologies. Specifically, we selected the two principal components related to the presence of two outstanding geological features of the volcanic rocks, iron oxides, and hydroxyl-bearing minerals (hydrothermal alteration).

Table 2 gives the eigenvector loadings obtained by PCA from the covariance matrix of the original image. PC1 presents similar positive weights for all the bands, except the TM5 band which presents a greater weight due to its greater variance depending on the gain and offset parameters of the sensor. This component is related to the albedo of the image, a factor which is responsible for the high correlation between the multispectral channels (Loughlin, 1991). The remaining PCs therefore account for the spectral differences between bands: PC2 represents the differences between the visible and the infrared, with high values corresponding to a high infrared reflectance; and low ones related to a high visible reflectance; PC3 provides information on iron oxides with a high weight in TM1 and a low one in TM3; and PC4 presents a high weight in the TM5 band and a low one for TM7, which suggests hydroxyl-bearing minerals. Summarizing all of the above, we can state that iron oxides and hydroxyls are mapped into PC3 and PC4, respectively.

The decision process for of the above six-band PCAs is a long and complex one because analysis of all the TM bands does not unequivocally separate the iron oxides and the hydroxyls into a simple PC image. As observed by Crosta and McMoore (1989), if the number of input channels is reduced, the chance of defining a unique PC for a specific mineral class will be increased. Consequently, we have decided to select two groups of bands representing each of the above-mentioned geological factors. In this sense, the TM1, TM3, TM4, and TM5 bands were chosen for the iron oxide analysis (Group 1), and the TM3, TM4, TM5, and TM7 bands for the analysis of hydroxyl-bearing minerals (Group 2).

In Group 1, the spectral contrast of the iron oxides is increased by omitting one mid-infrared band, which is sensitive to the presence of alteration minerals. Similarly, in order to highlight the alteration minerals, Group 2 omits two bands from the visible, i.e., those that demonstrate the presence of iron oxides.

TABLE 2. EIGENVECTOR LOADINGS OF THE PRINCIPAL COMPONENTS OF THE SIX TM BANDS

	PC1	PC2	PC3	PC4	PC5	PC6
TM1	0.3606	−0.5708	0.6609	0.0033	0.1828	0.2719
TM2	0.2600	−0.3116	−0.0203	−0.0866	−0.0609	−0.9076
TM3	0.3941	−0.3217	−0.4391	−0.2394	−0.6340	0.2986
TM4	0.3521	−0.1809	−0.5313	0.5321	0.5196	0.0891
TM5	0.6289	0.6104	0.2705	0.3096	−0.2459	−0.0485
TM7	0.3572	0.2614	−0.1206	−0.7458	0.4801	0.0542

Table 3. Eigenvector Loadings of the Principal Components of the Two Groups of TM Bands

	Group 1: Iron oxide					Group 2: Hydroxyl			
	PC1	PC2	PC3	PC4		PC1	PC2	PC3	PC4
TM1	0.4039	−0.6166	0.6549	−0.1665	TM3	0.4024	−0.6810	0.2769	−0.5455
TM3	0.4384	−0.3485	−0.4163	0.7162	TM4	0.3690	−0.4818	−0.4928	0.6236
TM4	0.3941	−0.1881	−0.5923	−0.6771	TM5	0.7312	0.5267	−0.3272	−0.2843
TM5	0.6995	0.6804	0.2165	0.0288	TM7	0.4089	0.1631	0.7572	0.4824

Table 3 gives the results of the PCAs for bands of the two groups, showing the weights of the eigenvectors obtained for each component. The methodology for iron oxide mapping by PCA is to examine the eigenvector loadings for the TM1 and TM3 bands; such loadings will be moderate to strong for both bands; and their signs will be reversed, which, indeed, is observed in PC3 of Group 1. The rule for hydroxyl mapping is similar to the previous one, i.e., the magnitude of eigenvector loadings for TM5 and TM7 should be moderate to strong and opposite in sign, which is observed in PC3 of Group 2.

As a conclusion to this analysis, the PC3s of each group of bands were chosen due to their significant relationship with the outcropping lithologies in the study area. Thus, besides the TM radiometric information, these two new variables are available, and can then be spatially analyzed by means of the methodology described.

Application of MSV for Lithologic Discrimination

Lacaze *et al.* (1994) have shown that the variogram function can be used for quantifying spatial variability of the radiometric data, revealing that each class or object in the image has a different spatial variability pattern. From one point of view, this pattern can be considered a "spatial variability signature" of the class. To show this previous aspect before calculating the MSV, different training areas for the six lithologies were variographically analyzed using the two selected PC3s. Experimental computation was performed by a computer program developed in our laboratory which allows us to define parameters such as direction, maximum distance, lag spacing, variogram type, and even variogram fitting. Figure 2 represents the omnidirectional variogram for the PC3s of the six lithologies at a lag spacing of one pixel (30 m). In general terms, the variograms reveal different spatial behavior of the lithologies with respect to their sill and range parameters: The ranges represent the spatial correlation of the variables and vary from low values, less than 100 m in the reef limestone, to high ones, around 300 m in the case of the amphibole dacite. The sill (variance) presents marked differences between the lithologic classes: the reef limestone and amphibole andesite present low sills, whereas the amphibole dacite and rhyolite are more heterogeneous and present a greater variance, although spatially they are a little more continuous.

These differences observed in the spatial variability patterns of the lithologic classes, some of which have a similar composition, are not only due to the mineralogy but also to the structural and textural aspects related to the processes of their formation. Thus, for example, the amphibole dacite outcropping as massive rocks (domes) show a greater spatial correlation (range) than do the amphibole andesite formed by autoclastic breccia of little extent. Also noteworthy is the similarity, in relative terms, of the variograms of the two PC3s, probably due to the high correlation between them.

These results show that the spatial variability of the radiometric data quantified by the variogram function can be used for lithologic discrimination purposes.

MSV Calculation and Discriminant Analysis

In order to add the spatial variability information to the classification strategy, the geostatistical measures of spatial variability were calculated on the PC3s using a moving window of 7 by 7 pixels and assigning the MSV values to the middle pixel. This window size gave the best results in the tests performed. The calculated uni- and multivariate MSV were direct variogram (V), madogram (M), rodogram (R), cross variogram (CV), and pseudo-cross variogram (PV), and their values were used only for the lag spacing of one pixel (30 m) as the average of the respective functions for the main directions (N-S, E-W, N45E, and N45W). Although in this case study a unique lag spacing was selected, which shows the best separability between classes, the method could also be applied by adding other values for different lag spacings, whenever the size of the window allows it.

As a result of this process, eight new variables were ob-

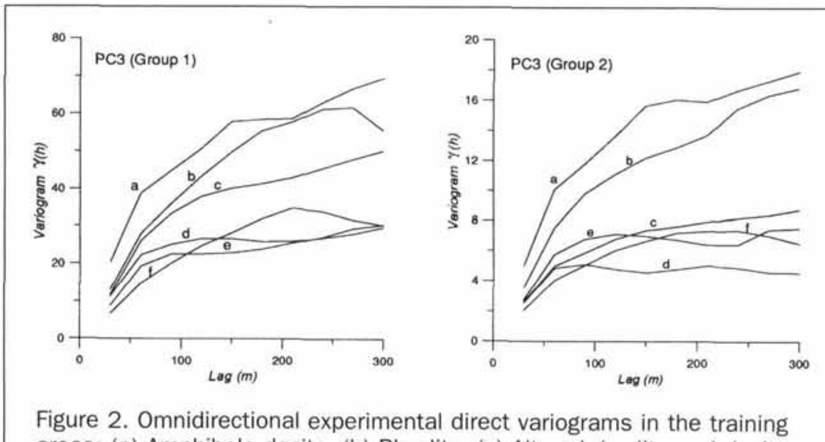

Figure 2. Omnidirectional experimental direct variograms in the training areas: (a) Amphibole dacite, (b) Rhyolite, (c) Altered rhyolite and dacite, (d) Reef limestone, (e) Amphibole andesite, and (f) Quaternary deposits.

Table 4. Results of Discriminant Analysis in the Lithologic Classification: TM (Thematic Mapper Bands), V (Variogram), M (Madogram), R (Rodogram), CV (Cross Variogram), PV (Pseudo-Cross Variogram) and σ^2 (variance)

Combination of variables	# variables	overall accuracy (%)	Combination of variables	# variables	overall accuracy (%)
TM	6	41.0	TM+CV	7	48.8
TM+σ^2	8	47.0	TM+PV	7	51.2
TM+V	8	42.8	TM+CV+PV	8	54.2
TM+M	8	52.4	TM+CV+PV+M	10	62.6
TM+R	8	52.4	TM+CV+PV+R	10	62.6
TM+V+M+R	12	53.6	TM+CV+PV+M+σ^2	12	63.3
TM+σ^2+V+M+R	14	60.8	TM+CV+PV+M+V	12	65.7

tained: six univariate measures, three for each PC3, and two multivariate ones corresponding to the two cross variograms of the PC3s. This may seem a high number of complementary variables and, indeed, they probably contain redundant information. To select the most relevant measures of variability, discriminant analysis was performed on a set of 41 training areas representing the six lithologies. For each pixel of these training areas, 16 variables were available: the six TM bands, the eight calculated MSV, and the two values of the statistical variance (σ^2) calculated on the PC3s in the moving windows. The use of the variance instead of the standard deviation is because the geostatistical expressions are mainly quadratic.

Different combinations of the above variables were studied to obtain the classification functions by standard discriminant analysis using the Statistica program (Statsoft, 1993). As the "truth," it considered sampled ground points located in the training areas. The results are summarized in Table 4, which includes the percentages of correctly classified pixels for the most significant combinations of the variables. Two important points are evident: first, the joint use of spectral and spatial information (TM bands and MSV, respectively) leads to a noteworthy increment in the rates of successful classifications; and second, the incorporation of the multivariate measures (CV and PV) plays an important role in improving the results, equivalent to those obtained from the univariate measures (V, M and R). It might also be mentioned that the redundancy of information provided by the madogram and rodogram is due to the similarity of these functions. Another consideration is that the local variance also contributes to improving the results, especially when it is used jointly with the univariate measures of variability.

Supervised Classification: Maximum Likelihood Decision Rule

Along the lines of the results of discriminant analysis, the following combination of variables was chosen to classify the Landsat TM image: the six TM bands and six MSV, the direct variogram and madogram for each PC3, and the cross and pseudo-cross variograms between PC3s.

Table 5. Results of the Supervised Classification in the Training Areas Showing the Percentage of Pixels Correctly Classified From Just TM Data (TM) and Using Both TM Data and the Best Combination of the Measures of Spatial Variability (TM+MSV)

Lithology	# pixels by classes	overall accuracy with TM (%)	overall accuracy with TM+MSV (%)	improvement (%)
Amphibole dacite	309	72.2	94.8	31
Amphibole andesite	190	56.3	85.3	51
Rhyolite	116	87.1	90.5	4
Altered rhyolite and dacite	150	87.3	99.3	14
Reef limestone	475	77.1	90.7	18
Quaternary deposits	570	77.4	91.9	19
Total	***1810***	***75.6***	***91.9***	***21***

In the study area, 41 training areas of similar size, covering 3 percent of the total surface area, were selected to define the spectral signature of the lithologies in which the ground truth was known. We compared the classification results obtained from a classical procedure, using only TM data, with the results derived from the proposed methodology, using jointly TM and MSV data. In both cases the maximum-likelihood decision rule was employed, expressed in the following equation (Erdas, 1997):

$$D = \ln(a_c) - [0.5 \ln(|\mathbf{Cov}_c|)] - [0.5(\mathbf{X} - \mathbf{M}_c)^T (\mathbf{Cov}_c^{-1})(\mathbf{X} - \mathbf{M}_c)] \quad (7)$$

where D is the weighted distance of a class, c is a particular class, $\mathbf{X}$ is the vector of measures of the candidate pixel, $\mathbf{M}_c$ is the mean of samples of class c, a_c is the *a priori* probability that a pixel candidate will belong to class c, $\mathbf{Cov}_c$ is the matrix of covariance of the pixels in the sample from class c, $|\mathbf{Cov}_c|$ is the determinant of $\mathbf{Cov}_c$, $\mathbf{Cov}_c^{-1}$ is the inverse of $\mathbf{Cov}_c$, ln is the natural logarithm, and T is the transposition function.

Table 5 gives the percentages of pixels correctly classified in the training areas for both classification cases. The increment in the success rate is very acceptable, as was foreseeable from the results of discriminant analysis. The improvements in the results of the classification vary depending on the lithologic class being considered. The improvements ranged from 51 percent for amphibole andesite to only 4 percent for the rhyolite, giving an average increment of around 20 percent. The extreme values are surprising, and we suppose they are due to the physical and textural characteristics of these outcropping rocks.

It may be seen from the results obtained in the supervised classification incorporating the measures of spatial variability that not only does the success rate increase but the classification also seems more homogeneous (Figure 3).

Discussion and Conclusions

Radiometric information from Landsat TM images is often used exclusively in digital classification, without considering other features of interest such as the spatial autocorrelation or variability of pixels within a local context. The use of this additional information improves remarkably the classification results. In this study, the classification was improved 51 percent compared by our methodology to the results obtained by classical methods.

The presented approach has been applied to lithologic mapping, from which the spectral enhancement of the main geological features of the outcropping materials—iron oxides and hydroxyl-bearing minerals—must be performed previously. To achieve this, the FPCS method was used to select one principal component representative of each of these geological features (PC3 in both cases). Variographic analysis performed in the training areas on these two components showed differences in the radiometric spatial patterns of the lithologies, even when some of them presented a similar petrological composition, due to the influence of the structural and textural features of the outcropping.

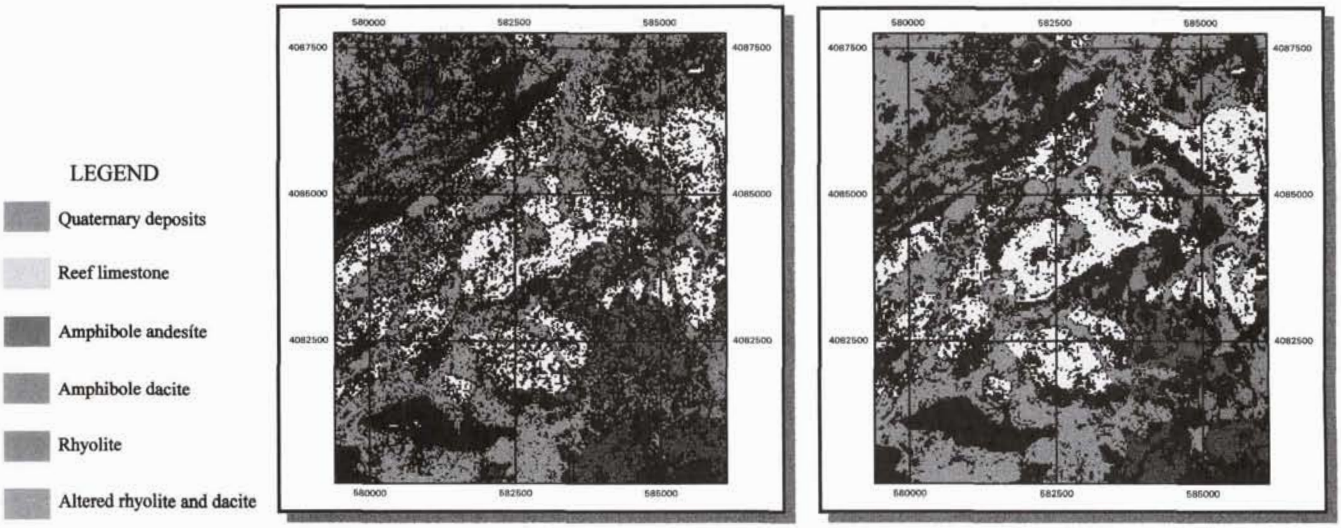

(a) (b)

Figure 3. Classification images of the Cabo de Gata study area applying the maximum-likelihood decision rule considering (a) just the Landsat TM multispectral information and (b) Landsat TM data and the best combination of the measures of spatial variability (variogram, madogram, cross variogram, and pseudo-cross variogram) calculated within a moving window of 7 by 7 pixels for the lag spacing of one pixel. The black class corresponds to misclassified pixels and non classified lithologies.

The proposed measures of spatial variability are based on different uni- and multivariate estimators of the variogram function, and were calculated in a neighborhood over the PC3s at the specific lag spacing of one pixel. Both window size and lag spacing were experimentally checked and selected for this specific application; in particular, we note that other lags can be used separately or jointly.

The evaluation of these geostatistical measures was carried out by discriminant analysis in the training areas. From this analysis, it was verified that the joint use of TM radiometric information and MSV improves the results, in agreement with established hypotheses. The best lithologic discrimination was obtained using jointly the TM data, the variogram and madogram for each PC3, and the cross and pseudo-cross variograms between these principal components, reaching an average increment in accuracy of around 20 percent. The improvement in the visual aspect concerning the class spatial homogeneity was also noteworthy.

We can conclude that measures of spatial variability should be considered for lithologic discrimination purposes, as they provide useful context information and they improve considerably the results obtained by the classical methodologies.

Acknowledgments

This paper was made possible thanks to the financial support of Brite/Euram Programme of the EC (Contract BRE2-CT93-0513) and the DGICYT under grant PB92-0925-CO2-02. We would also like to thank the anonymous referees for providing positive comments.

References

Abarca-Hernández, F., 1997. *Desarrollo de técnicas geoestadísticas en el tratamiento de imágenes de teledetección*, doctoral thesis, University of Granada, 330 p.

Arribas, A., Jr., J.J. Rytuba, R.O. Rye, C.G. Cunningham, M.H. Podwysocki, W.C. Kelly, A. Arribas, E.H. McKee, and J.G. Smith, 1989. *Preliminary Study of the Ore Deposits and Hydrothermal Alteration in the Rodalquilar Caldera Complex, Southeastern Spain*, U.S. Geological Survey Open-File Report 89-327, 39 p.

Atkinson, P.M., 1993. The effect of spatial resolution on the experimental variogram of airborne MSS imagery, *Int. J. of Remote Sensing*, 14:1005–1011.

Atkinson, P.M., R. Webster, and P.J. Curran, 1994. Cokriging with airborne MSS imagery, *Remote Sensing of Environment*, 50:335–345.

Carr, J.R., 1996. Spectral and textural classification of single and multiple band digital images, *Computer and Geosciences*, 22: 849–865.

Carlson, G.E. and W.J. Ebel, 1995. Co-ocurrence matrices for small region texture measurement and comparison, *Int. J. Remote Sensing*, 16:1417–1423.

Chica-Olmo, M., and F. Abarca, 1998. Radiometric coregionalization of Landsat TM and SPOT HRV images, *Int. J. Remote Sensing*, 19:997–1006.

Clarke, C.K., 1986. Computation of the fractal dimension of topographic surfaces using the triangular prism surface area method, *Computer and Geosciences*, 12:713–722.

Cressie, N.A.C., 1993. *Statistics for Spatial Data*, John Wiley & Sons, New York, 900 p.

Crosta, A.P., and J. McMoore, 1989. Enhancement of Landsat Thematic Mapper imagery for residual soil mapping in sw Minas Gerias state, Brazil: A prospecting case history in Greenstone Belt terrain, *Proccedings of the 7th (ERIM) Thematic Conference: Remote Sensing for Exploration Geology*, Calgary, pp. 1173–1187.

Curran, P.J., 1988. *The semivariogram in remote sensing: An introduction, Remote Sensing of Environment*, 24:493–507.

Deutsch, C.V., and A.G. Journel, 1992. *GSLIB. Geostatistical Software Library and User's Guide*, Oxford University Press, New York, 340 p.

Dungan, J.L., D.L. Peterson, and P.J. Curran, 1994. Alternative approaches for mapping vegetation quantities using ground and image data, *Enviromental Information Management and Analysis: Ecosystem to Global Scale* (W. Michener, J. Brunt, and S. Stafford, editors) Taylor & Francis, London, pp. 237–261.

Erdas Imagine, 1997. *Erdas field guide, Release 8.3*, (Erdas Inc., Atlanta, Georgia), 656 p.

Haralick, R.M., and K.S. Shanmugham, 1974. Combined spectral and spatial processing of ERTS imagery data, *Remote Sensing of Environment*, 3:3–13.

Journel, A.G., and C.J. Huijbregts, 1978. *Mining Geostatistics*, Academic Press, London, 600 p.

Lacaze, B., S. Rambal, and T. Winkel, 1994. Identifying spatial patterns of Mediterranean landscapes from geostatistical analysis of remotely-sensed data, *Int. J. Remote Sensing*, 15:2437–2450.

Lark, R.M., 1996. Geostatistical description of texture on an aerial photograph for discriminating classes of land cover, *Int. J. Remote Sensing*, 17:2115–2133.

Loughlin, W.P., 1991. Principal component analysis for alteration mapping, *Photogrammetric Engineering & Remote Sensing*, 57: 1163–1169.

Matheron, G., 1965. *Les variables Régionalisées et leur Estimation*, Masson, Paris, 306 p.

———, 1971. *The Theory of Regionalized Variables and its Applications*, Centre de Morphologie Mathématique de Fontainebleau, Fontainebleau, 211 p.

———, 1982. *La Destructuration des hautes teneurs et le krigeage des Indicatrices*, Centre de Morphologie Mathématique de Fontainebleau, N-761, Fontainebleau, 33 p.

McBratney, A.B., and R. Webster, 1986. Choosing functions for semi-variograms of soil properties and fitting them to sampling estimates, *Journal Soil Science*, 37:617–639.

Ramstein, G., and M. Raffy, 1989. Analysis of the structure of radiometric remotely-sensed images, *Int. J. of Remote Sensing*, 10: 1049–1073.

Statsoft, Inc., 1993. *Statistica Reference Manual, Release 4*, Statsoft Inc., Tulsa, Oklahoma, xxx p.

Sun, X.H., and P. Qin, 1993. Texture analysis for remotely sensed imagery, *Proceedings of the Ninth Thematic Conference on Geological Remote Sensing*, 1:311–322.

Swain, P., H. Siegel, and B. Smith, 1979. A method for classifying multispectral remote sensing data data using context, *1979 Machine Processing of Remotely Sensed Data Symposium*.

Wackernagel, H., 1995. *Multivariate Geostatistics*, Springer-Verlag, Berlin, 256 p.

Woodcock, C.E, A.H. Strahler, and D.L.B. Jupp, 1988. The use of variograms in remote sensing: II. Real digital images. *Remote Sensing of Environment*, 25:349–379.

(Received 30 June 1997; revised and accepted 30 July 1998; revised 09 September 1998)